Functional Nanoparticles

DOI: 10.1002/anie.200802323

Hollow Manganese Oxide Nanoparticles as Multifunctional Agents for Magnetic Resonance Imaging and Drug Delivery**

Jongmin Shin, Rahman Md Anisur, Mi Kyeong Ko, Geun Ho Im, Jung Hee Lee, and In Su Lee**

Nanometer-sized colloidal particles with small size and large surface area have many superior properties when used as magnetic resonance imaging (MRI) contrast agents, such as their ability to carry large payloads of active magnetic centers, easy penetration of biological membranes, long blood circulation times, and efficient conjugation to affinity molecules. Thus, they have the potential to allow us to visualize targets at low imaging-agent concentration with high sensitivity and sepcificity.[1] Furthermore, nanoparticles can be used in combination with therapeutic agents as bifunctional medical systems that enable simultaneous MRI diagnosis and drug treatment.[2] For example, superparamagnetic iron oxide nanoparticles have been developed as efficient T_2 contrast agents and employed to image tumors, stem cell migration, and cancer metastases.[3] Some colloidal nanoparticles containing gadolinium(III) or manganese(II) have recently been reported as potent T_1 MRI contrast agents.[4] Very recently, some of the present authors developed MnO nanoparticles as T_1 contrast agents for MRI signal enhancement of the anatomic brain structure.[5]

The further development of nanoparticle MRI contrast agents will require materials with higher relaxivity than the current state of the art that can operate at much lower concentrations of potentially toxic metal ions such as Gd^{3+} and Mn^{2+}. In this context, hollow nanoparticles with interior void spaces are attractive candidates owing to their large water-accessible surface areas, which are able to carry high payloads of MR-active magnetic centers, and because they can take up a large amount of therapeutic drug within the interior void.[6] While hollow nanoparticles containing magnetic ions have recently been prepared through several synthetic strategies, there are few examples of the investigation of their medical applications.[7]

Herein, we report a novel and facile synthesis of hollow manganese oxide nanoparticles (HMONs) and their potential application as multifunctional agents for simultaneous MR imaging and drug delivery. We demonstrate the greatly improved relaxivities of the hollow nanoparticles along with their efficient cellular uptake and drug loading capacities. These properties allow us to develop these particles for the delivery of therapeutic drugs as well as for diagnostic imaging.

Manganese oxide nanoparticles with a diameter of 20 nm stabilized by oleic acid (MONs) as well as water-dispersible manganese oxide nanoparticles (WMONs) were prepared using a reported procedure involving the thermal decomposition of a manganese oleate complex and encapsulation with poly(ethylene glycol) phospholipid.[5] The powder X-ray diffraction (XRD) patterns revealed that MnO is the main component of both MONs and WMONs and showed an increase of the Mn_3O_4 fraction in the WMONs. The analysis of the surface composition with X-ray photoelectron spectroscopy (XPS) indicated the presence of Mn^{II} and Mn^{III} (see the Supporting Information). On the basis of these observations, it was presumed that the as-synthesized MONs were passivated with Mn_3O_4 formed by their contact with air, even under an organic solvent, and that further oxidation occurred to form a thicker Mn_3O_4 shell when they were transferred into water. Very recently, the oxidation of the surface of MnO nanoparticles in air was also reported.[8]

The hollow interior of the HMONs was created by selective removal of the core MnO phase from the WMONs in acidic solution (Scheme 1). After being stirred at room temperature for 12 h in phthalate buffer solution at pH 4.6, the HMONs were separated from the light brown supernatant solution and washed with distilled water several times. The suspension of purified HMONs exhibited good colloidal stability, suggesting that there was no disruption of the coating by the surfactant molecules.

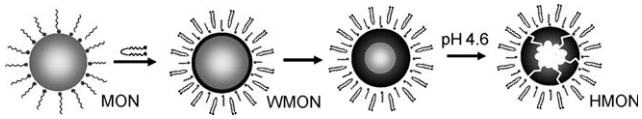

Scheme 1. Formation of HMONs. MnO gray, Mn_3O_4 black. ⟿: oleate. ⟿: poly(ethylene glycol) phospholipid.

Transmission electron microscopy (TEM) and scanning electron microscopy (SEM) revealed the formation of HMONs having interior voids and size distributions similar to the starting WMONs. After repeated experiments, it was

[*] M. K. Ko, G. H. Im, Prof. J. H. Lee
Department of Radiology, Samsung Medical Center
Sungkyunkwan University School of Medicine
Seoul 135-710 (Korea)
Fax: (+82) 2-3410-0084
E-mail: hijunghee@skku.edu
J. Shin, R. M. Anisur, Prof. I. S. Lee
Department of Chemistry & Advanced Material Sciences
Kyung Hee University, Gyeonggi-do 446-701 (Korea)
E-mail: insulee97@khu.ac.kr

[**] This work was supported by a Korea Research Foundation Grant funded by the Korean Government (MOEHRD) (KRF-2007-331-C00145). J.H.L. is supported by the Center for Biological Modulators of the 21st Century Frontier R&D Program (CBM31-B3002-00-00-00). We thank Prof. Jungahn Kim at Kyung Hee University for his kind donation of doxorubicin.

Supporting information for this article is available on the WWW under http://dx.doi.org/10.1002/anie.200802323.

revealed that the prolonged immersion of the WMONs in water before the acid treatment brought about remarkable changes in the interior shape of the resulting HMONs (Figure 1). Immersion of WMONs in water for one day afforded an interior cavity with roughly spherical shape and a diameter of 12 nm. High-resolution TEM (HRTEM) images of these HMONs show open cavities imperfectly surrounded by multiple crystalline domains. Increasing the immersion time yielded closed cavities; the hollow cavities in HMONs obtained after immersion in water for five days were completely surrounded by polycrystalline shells. The inner surface was found to be highly wrinkled, which contributes to the large surface area of the hollow nanoparticles. HRTEM analyses also revealed that immersion for 10–40 days yielded two or three irregularly shaped cavities having average diameters of 8–5 nm within a resulting HMON particle.

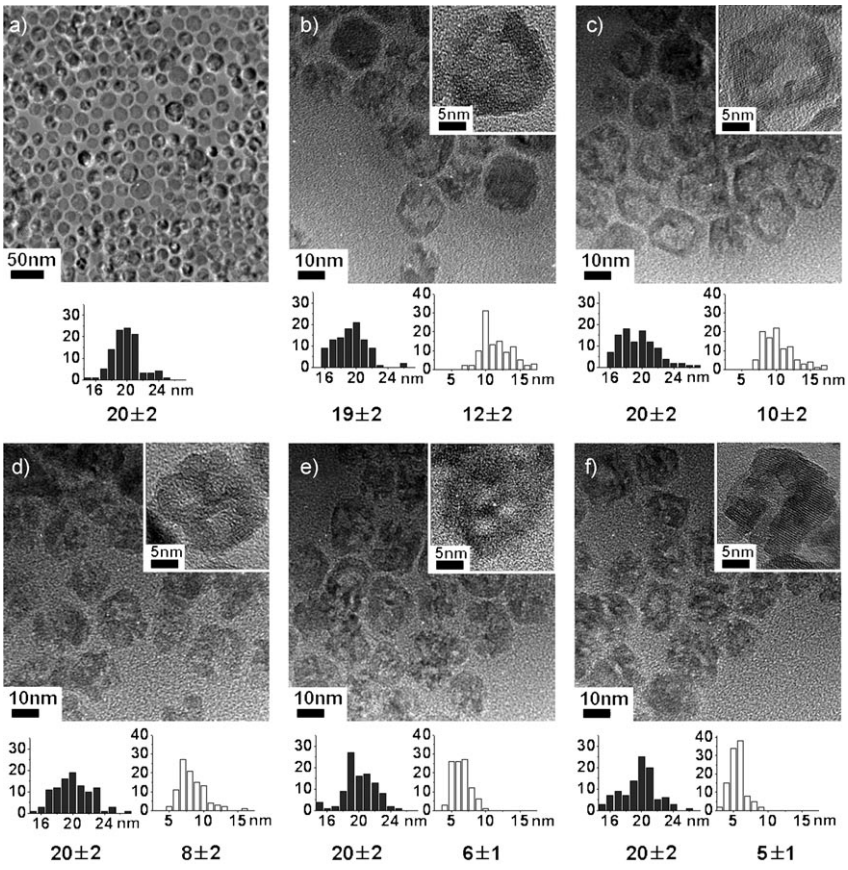

Figure 1. TEM images of a) WMONs and b–f) HMONs prepared after immersion in water for 1 (b), 5 (c), 10 (d), 20 (e), and 40 days (f), showing the evolution of the interior structure of resulting HMONs depending on the duration of immersion. Histograms show the size distribution of the external diameter (grey bars) and interior cavity (white bars) of the nanoparticles.

The XRD pattern of HMONs prepared after immersion in water for five days shows broad peaks, reflecting the polycrystalline nature of the particles, and a marked decrease of the MnO fraction, which indicates the preferential dissolution of the MnO phase at the core and the stability of the Mn_3O_4 shell phase under the acidic reaction conditions (Figure 2a). The HMONs showed ferromagnetic behavior at low temperature, while they were paramagnetic at around room temperature, which also supports the conclusion that they are composed mainly of Mn_3O_4 (Figure 2b).[9] The smaller cavities may form with longer duration of water immersion because most of the MnO phase was converted into Mn_3O_4 in the starting WMONs.

To evaluate the effectiveness of the nanoparticles as MRI agents, the relaxation properties of WMONs and of HMONs prepared by five-day immersion were examined using a 3.0 T human clinical scanner. As shown in Figure 3, the HMONs exhibited much stronger enhancement in both T_1- and T_2-weighted MRI than the WMONs at the same Mn concentration. The specific relaxivities, obtained by measuring the relaxation rate as a function of the concentration of the contrast agent, were found to be markedly increased for the HMONs as compared to the WMONs. The r_1 and r_2 values of the HMONs were 7.0 and 5.5 times higher, respectively, than those of the WMONs when calculated on the basis of the concentration of Mn ions, and they were 5.8 and 4.4 times higher when calculated on the basis of the nanoparticle concentration (Table 1). Although the exact explanation for this enhancement requires further research, it can be inferred that the increased relaxivities of the HMONs are mainly due to the increased concentration of Mn ions exposed at the hollow inner surface.

To assess the potential of the nanoparticles as drug delivery vehicles, their drug-loading capacity was investigated with a hydrophobic anticancer agent (doxorubicin, DOX). The nanoparticles were loaded with drug by mixing them with DOX in CH_3OH/CH_3Cl (1:7), evaporating the organic solvent, and transferring the residual material into water. As listed in Table 1, the amount of DOX incorporated into the HMONs (five-day immersion) was 3.5 times higher than that of the WMONs based on the concentration of Mn ions and 3.0 times higher based on the number of nanoparticles. This result demonstrates the potential utility of HMONs as efficient vehicles for targeted delivery of anticancer therapeutic agents through conjugation with targeting molecules. It could be hypothesized that hydrophobic DOX molecules would partition into the shells of oleic acid molecules surrounding the nanoparticle surface.[10] It can be inferred that owing to the highly wrinkled surface of the cavity wall, the inner surface area of the HMONs would be much larger than that of its spherical outer surface. Thus, the higher loading capacity of HMONs can be largely attributed to their larger surface area interacting with oleic acids.

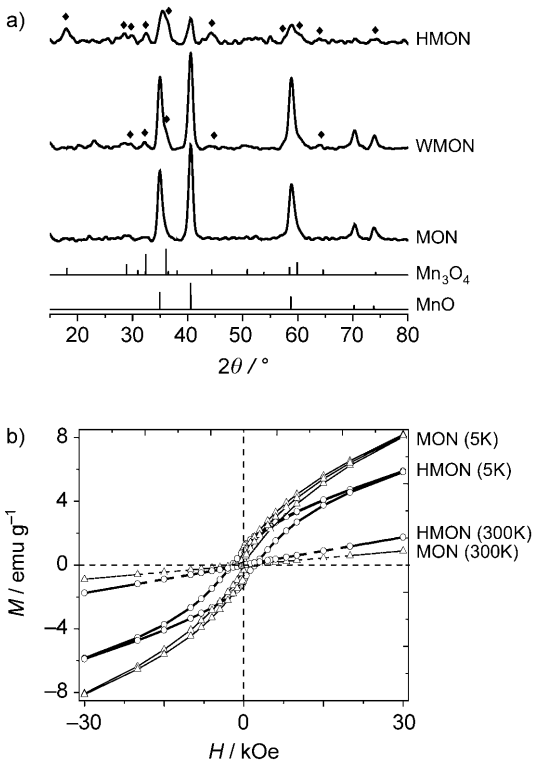

Figure 2. a) XRD patterns of MONs, WMONs, and HMONs. Peaks corresponding to Mn_3O_4 are marked with diamonds. The lines below show the position of the reflections corresponding to cubic MnO phase (JCPDS Card No. 07-0230) and the tetragonal Mn_3O_4 phase (JCPDS Card No. 24-0734). b) Hysteresis loops of MONs (△) and HMONs (○) at $T = 300$ K (dotted lines) and $T = 5$ K (solid lines).

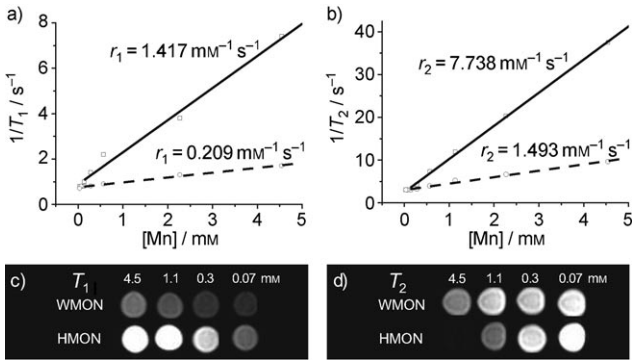

Figure 3. Plots of a) T_1^{-1} and b) T_2^{-1} versus Mn concentration for WMONs (dotted lines) and HMONs (solid lines). c) T_1- and T_2-weighted MRI results obtained from aqueous suspensions of WMONs and HMONs at various Mn concentrations.

Table 1: Relaxation and drug loading properties of the nanoparticles.

Nanoparticle	T_1[a] [ms]	T_2[a] [ms]	For the same manganese concentration			For the same nanoparticle concentration[c]		
			r_1 [s mM^{-1}]	r_2 [s mM^{-1}]	Dox load[b] [μg]	r_1 [s μM^{-1}]	r_2 [s μM^{-1}]	Dox load[d] [mg]
WMON	585	104	0.21	1.49	58	31	223	8.6
HMON	135	27	1.42	7.74	202	180	983	25.6

[a] Measured at 4.5 mM Mn (as measured by ICP AES). [b] Per 1 mg of Mn. [c] Derived by approximating the nanoparticles as hollow spheres. [d] Per 1 M nanoparticles.

The effectiveness of the HMONs for MR labeling and intracellular drug delivery was evaluated by examination of MCF-7 and MDA-MB-435s cells incubated with DOX-loaded HMONs. Confocal laser scanning microscopy (CLSM) revealed that the DOX molecules associated with the HMONs were localized in the cytoplasm, whereas free DOX was mostly found in the cell nuclei, demonstrating the efficient internalization of the HMONs, which carried DOX into the cells within 2 h of incubation, most likely through the endocytosis mechanism (Figure 4a,b).

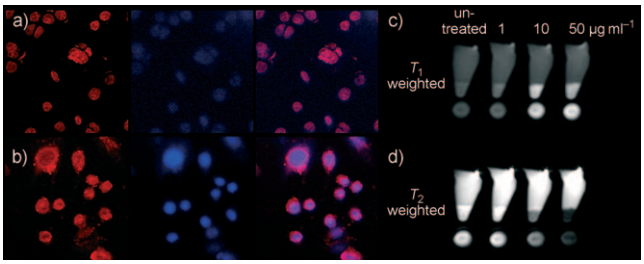

Figure 4. CLSM images of DOX fluorescence (left) and of the nuclei of cells stained by Hoechst 33342 (middle) and a merged image (right) for MDA-MB-435s cells incubated a) with free DOX and b) with DOX-loaded HMONs at 10 μM DOX concentration for 2 h. c) T_1-weighted and d) T_2-weighted MRI images of MCF-7 cells incubated in media with DOX-loaded HMONs at various concentrations for 2 h.

The in vitro cytotoxicity of DOX-loaded HMONs was evaluated on MCF-7 cell lines and compared with that of free DOX. HMONs alone did not show any significant cytotoxicity under experimental conditions. DOX-loaded HMONs, however, showed a dose-dependent cytotoxic effect, which was slightly smaller than that observed with equivalent doses of DOX in solution (see the Supporting Information). This finding could stem from the sustained drug release of the HMONs. Furthermore, concentration-dependent signal enhancement was observed in the MRI images of MCF-7 cells treated with DOX-loaded HMONs compared with a control sample of untreated cells. This result confirms that HMONs are efficiently labeled for MRI. Interestingly, significant contrast enhancement was found in both the T_1- and T_2-weighted images. As shown in Figure 4c,d, a significant bright contrast in the T_1-weighted MRI image and a dark contrast in the T_2-weighted image were found as the concentration of DOX-loaded HMONs increased. The dual contrast enhancement was also confirmed by in vivo MRI images of a mouse brain that was locally injected with 1 μL HMON solution (2.21 μg Mn measured by inductively coupled plasma atomic emission spectroscopy (ICP-AES)) one hour prior to imaging (Figure 5a,b). The T_1- and T_2-weighted MRI images of the mouse brain revealed bright signal enhancement and a dark signal void, respectively, in the region where the HMONs were locally injected, demonstrating the unique potential of these particles as a dual contrast agent for both T_1-

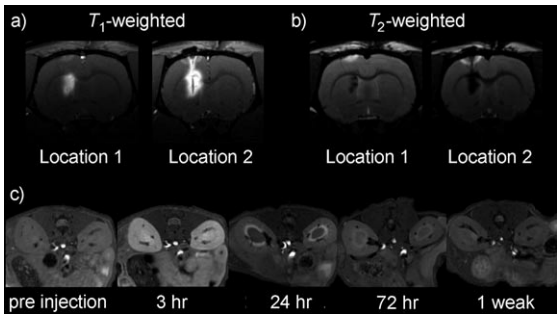

Figure 5. a) T_1- and b) T_2-weighted MRI images of a mouse brain that was locally injected with HMONs: two locations were compared in T_1- and T_2-weighted MRI images. c) A time course of the signal enhancement in T_1-weighted MRI of a mouse kidney after intravascular injection of HMONs.

and T_2- weighted MRI. When HMONs (10 mg of Mn measured by ICP-AES per kilogram of mouse body weight) were intravascularly administrated to a mouse through a tail vein, a time course of signal enhancement was clearly observed in T_1-weighted imaging of the kidney, indicating the utility of HMONs as intravascular MRI contrast agents (Figure 5c).

In summary, we developed a method of synthesizing hollow manganese oxide nanoparticles and confirmed the superiority of their MRI contrast efficiency and drug-loading capacity. We demonstrated their effectiveness in labeling for MRI and intracellular drug delivery. We also demonstrated their potential utility as a dual contrast agent for T_1- and T_2-weighted MRI. We believe that the results of the current study will provide a novel approach for developing bifunctional MRI agents combining diagnostic imaging and targeted delivery of therapeutic agents.

Experimental Section

Synthesis of HMONs and DOX-loaded HMONs: WMONs were prepared by the reported method with some modifications.[5] The WMONs were dispersed in distilled water and stored several days. WMONs (10 mg) were dispersed into phthalate buffer (20 mL, pH 4.6) and stirred for 12 h to carve away the MnO core. Resulting HMONs were retrieved by ultracentrifugation and washed several times by repeated dispersion in distilled water and ultracentrifugation. The solid HMONs (1.57 mg) were dispersed into methanol/choloroform (1:7) containing DOX (1 mg) in the presence of a small amount of oleic acid. After the evaporation of the solvent, water (2 mL) was added, resulting in an aqueous dispersion of DOX-loaded HMONs. Unloaded DOX was removed by repeated ultracentrifugation and redispersion in distilled water.

Received: May 19, 2008
Revised: October 6, 2008
Published online: November 28, 2008

Keywords: contrast agents · drug delivery · magnetic resonance imaging · manganese · nanoparticles

[1] a) J. W. M. Bulte, D. L. Kraitchman, *NMR Biomed.* **2004**, *17*, 484; b) S. Mornet, S. Vasseur, F. Grasset, E. Duguet, *J. Mater. Chem.* **2004**, *14*, 2161.

[2] a) J. Kim, J. E. Lee, S. H. Lee, J. H. Yu, J. H. Lee, T. G. Park, T. Hyeon, *Adv. Mater.* **2008**, *20*, 478; b) J. Yang, C.-H. Lee, H.-J. Ko, J.-S. Suh, H.-G. Yoon, K. Lee, Y.-M. Huh, S. Haam, *Angew. Chem.* **2007**, *119*, 8992; *Angew. Chem. Int. Ed.* **2007**, *46*, 8836; c) N. Nasongkla, E. Bey, J. Ren, H. Ai, C. Khemtong, J. S. Guthi, S.-F. Chin, A. D. Sherry, D. A. Boothman, J. Gao, *Nano Lett.* **2006**, *6*, 2427.

[3] a) C. Xu, J. Xie, D. Ho, C. Wang, N. Kohler, E. G. Walsh, G. R. Morgan, Y. E. Chin, S. Sun, *Angew. Chem.* **2008**, *120*, 179; *Angew. Chem. Int. Ed.* **2008**, *47*, 173; b) J. Lee, Y.-M. Huh, Y. Jun, J. Seo, J. Jang, H. Song, S. Kim, E. Cho, H. Yoon, J. Suh, J. Cheon, *Nat. Med.* **2007**, *13*, 95; c) I. J. M. de Vries, W. J. Lesterhuis, J. O. Barentsz, P. Verdijk, J. H. van Krieken, O. C. Boerman, W. J. G. Oyern, J. J. Bonenkamp, J. B. Boezeman, G. J. Adema, J. W. M. Bulte, T. W. J. Scheene, C. J. A. Punt, A. Heerschap, C. G. Figdor, *Nat. Biotechnol.* **2005**, *23*, 1407; d) M. G. Harisinghani, J. Barentsz, P. F. Hahn, W. M. Deserno, S. Tabatabaei, C. H. van de Kaa, J. de La Rosette, R. Weissleder, *N. Engl. J. Med.* **2003**, *348*, 2491.

[4] a) K. M. Taylor, J. S. Kim, W. J. Rieter, H. An, W. Lin, W. Lin, *J. Am. Chem. Soc.* **2008**, *130*, 2154; b) J.-L. Bridot, A.-C. Faure, S. Laurent, C. Rivière, C. Billotey, B. Hiba, M. Janier, V. Josserand, J.-L. Coll, L. V. Elst, R. Muller, S. Roux, P. Perriat, O. Tillement, *J. Am. Chem. Soc.* **2007**, *129*, 5076; c) S. Wang, B. R. Jarrett, S. M. Kauzlarich, A. Y. Louie, *J. Am. Chem. Soc.* **2007**, *129*, 3848; d) W. J. Rieter, K. M. Taylor, H. An, W. Lin, W. Lin, *J. Am. Chem. Soc.* **2006**, *128*, 9024; e) H. Hifumi, S. Yamaoka, A. Tanimoto, D. Citterio, K. Suzuki, *J. Am. Chem. Soc.* **2006**, *128*, 15090; f) S. Flacke, S. Fischer, M. J. Scott, R. J. Fuhrhop, J. S. Allen, M. McLean, P. Winter, G. A. Sicard, P. J. Gaffney, S. A. Wickline, G. M. Lanza, *Circulation* **2001**, *104*, 1280.

[5] H. B. Na, J. H. Lee, K. An, Y. I. Park, I. S. Lee, D.-H. Nam, S. T. Kim, S.-H. Kim, S.-W. Kim, K.-H. Lim, K.-S. Kim, S.-O. Kim, T. Hyeon, *Angew. Chem.* **2007**, *119*, 5493; *Angew. Chem. Int. Ed.* **2007**, *46*, 5397.

[6] Synthesis of hollow sphere nanoparticles, a) X. Liang, X. Wang, Y. Zhuang, B. Xu, S. Kuang, Y. Li, *J. Am. Chem. Soc.* **2008**, *130*, 2736; b) Y. Yin, C. Erdonmez, S. Aloni, A. P. Alivisatos, *J. Am. Chem. Soc.* **2006**, *128*, 12671; c) X. Lu, H.-Y. Tuan, J. Chen, Z.-Y. Li, B. A. Korgel, Y. Xia, *J. Am. Chem. Soc.* **2007**, *129*, 1733; d) F. Caruso, *Colloids and Colloid Assemblies*; Wiley-VCH, Weinheim, **2003**; e) Y. Sun, B. Mayers, Y. Xia, *Adv. Mater.* **2003**, *15*, 641; f) F. Caruso, *Chem. Eur. J.* **2000**, *6*, 413; g) M. Han, J. Zhu, Y. Liang, Z. Xu, Y. Song, *Adv. Mater.* **2005**, *17*, 1995.

[7] Hollow nanoparticles containing magnetic metal ions, a) S. Peng, S. Sun, *Angew. Chem.* **2007**, *119*, 4233; *Angew. Chem. Int. Ed.* **2007**, *46*, 4155; b) A. E. Henkes, Y. Vasquez, R. E. Schaak, *J. Am. Chem. Soc.* **2007**, *129*, 1896; c) J. Gao, G. Liang, B. Zhang, Y. Kuang, X. Zhang, B. Xu, *J. Am. Chem. Soc.* **2007**, *129*, 1428; d) J. H. Gao, B. Zhang, X. X. Zhang, B. Xu, *Angew. Chem.* **2006**, *118*, 1242; *Angew. Chem. Int. Ed.* **2006**, *45*, 1220; e) A. H. Latham, M. J. Wilson, P. Schiffer, M. E. Williams, *J. Am. Chem. Soc.* **2006**, *128*, 12632; f) Y. Yin, R. N. Rioux, C. K. Erdonmez, S. Hughes, G. A. Somorjai, A. P. Alivisatos, *Science* **2004**, *304*, 711.

[8] a) A. E. Berkowitz, G. F. Rodriguez, J. I. Hong, K. An, T. Hyeon, N. Agarwal, D. J. Smith, E. E. Fullerton, *Phys. Rev. B* **2008**, *77*, 024403; b) G. Salazar-Alvarez, J. Sort, S. Suriñach, M. D. Baró, J. Nogués, *J. Am. Chem. Soc.* **2007**, *129*, 9102.

[9] W. S. Seo, H. H. Jo, K. Lee, B. Kim, S. J. Oh, J. T. Park, *Angew. Chem.* **2004**, *116*, 1135; *Angew. Chem. Int. Ed.* **2004**, *43*, 1115.

[10] T. K. Jain, M. A. Morales, S. K. Sahho, D. L. Leslie-Pelecky, V. Labhasetwar, *Mol. Pharmaceutics* **2005**, *2*, 194.

